Investigation of Additive Manufactured and Extruded Hard-Magnetic Rotors for Surface-Mounted Permanent Magnet Synchronous Machines

T. Wu[1], D. Schwarzer[1,2], A. Rüdiger[3], S. Gall[4], T. Neuwald[5], P. Wüst[5], D. Maczionsek[5], F. Seibicke[6], H. Rauch[6], K. Brach[6], U. Schäfer[1]

[1] Institute of Electrical Drive, Technische Universität Berlin, Berlin, Germany
[2] M-Pulse GmbH, Berlin, Germany
[3] Forschungszentrum Strangpressen, Technische Universität Berlin, Berlin, Germany
[4] INGWERK GmbH, Berlin, Germany
[5] Fraunhofer Institute for Production Systems and Design Technology IPK, Berlin, Germany
[6] Large Drives Applications, Siemens AG, Berlin, Germany

Abstract

The advancements in technology have led to a growing interest in additive manufacturing owing to its numerous benefits such as increased degree of freedom, high flexibility, and material conservation. It has gained particular attention in the production of electrical machines and their active components such as windings, electrical insulation, magnetic core packs, and permanent magnets. This paper investigates the use of three methods, namely fused deposition modeling, cold spray and extrusion, in the production of hard magnetic components for rotors with surface-mounted magnets. The produced magnets exhibit either isotropic behavior or an anisotropy in the radial direction, which results in significant improvements of motor performance, particularly in cogging torque and torque pulsation. A comparative study was conducted through a combination of finite element simulations and experimental tests.

1 Introduction

As a critical component in electrical machines, permanent magnets (PM) have been produced since the 18th century by powder metallurgy. This intricate process involves the mixing and preparation of powders and alloys, followed by pressing and aligning, and finally sintering and heat treatment [1]. However, despite the long production time and complexity of the process, the shape and anisotropic direction of the produced magnets are heavily constrained by the pressing and aligning stages, which restrict their applicability in various fields. Therefore, the implementation of additive manufacturing (AM) presents novel opportunities for designing electrical machines in the construction sector. It offers several key benefits, including rapid and cost-effective production, enhanced flexibility in the manufacturing process, and the ability to create lightweight structures [2].

In electrical machine applications, the key materials for magnets are Ferrite, NdFeB and SmCo. These magnets can be manufactured using additive processes such as selective laser melting, fused deposition modeling (FDM), and cold spray (CS) [3]. Goll *et al.* [4] successfully produced high-performance selective laser melting based NdFeB magnets and concluded that this technique enables the realization of very fine microstructures with defined texture. Another study on isotropic FDM-based magnets was carried out in [5], where a comparison was made with injection-molded magnets using the same material. Lamarre *et al.* [6] demonstrated the direct shaping of NdFeB composite material on electric motor parts using the CS method. The study showcased the promising potential of manufacturing magnets by fine-tuning the process parameters during the CS process. Furthermore, due to the advantages of AM, numerous studies have concentrated on the design process and soft-magnetic components of rotors using such as laser powder bed fusion or laser beam melting [7]-[9]. However, the existing studies were predominantly concentrated on either the manufacturing of hard-magnetic materials using a single method or the design process involving soft-magnetic materials for electrical machines.

Therefore, this paper explores three different methods for manufacturing hard-magnetic materials and compares their performance in electrical machines. Firstly, magnets were manufactured using the FDM, CS and extrusion (ET) methods, with a focus on generating anisotropic behavior. Secondly, demonstrators based on magnetic properties and corresponding magnetizing facilities were designed and simulated. Lastly, experimental investigations and comparisons were conducted on the demonstrators with AM-magnets.

2 Additive Manufacturing and Extrusion of Hard-Magnetic Materials

2.1 Fused Deposition Modelling (FDM)

FDM is one of the seven AM-methods according to EN ISO/ASTM 52921:2017 [10]. It belongs to the category of material extrusion and is widely recognized as one of the most popular technologies for rapidly prototyping products and conceptual models. In addtition to the general advantages of AM, the FDM stands out as an appealing choice for manufacturing of PM due to the simplified plant setup, flexible processing environment, and compatibility with magnetic materials.

A FDM machine tool was designed and built in an open coverage method at Fraunhofer IPK. **Fig. 1** illustrates the

functional principle and provides an overview of the facility. The rigid filament is fed to the hot end using extruder, where it undergoes melting. The viscous material is then printed layer by layer on the print bed through a nozzle. The resulting PM samples, also referred to as green parts, undergo further processing involving debinding, sintering and thermal treatment.
To produce anisotropy in the printed magnets, a magnetic field with about 0.8 T is generated around the nozzle's printing area using a Halbach-Array (HA) of Permanent magnets.

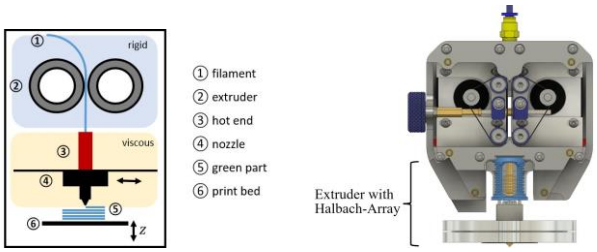

Figure 1: (a) Schematic representation and (b) developed extruder with HA of the fused deposition modeling method [2]

2.2 Cold Spray (CS)

Another promising AM-process for manufacturing of hard-magnetic materials is cold spray. Unlike laser-based processes such as laser powder bed fusion or laser powder buildup welding, the CS process operates without the need for thermal energy. Instead, it utilizes the kinetic energy of powder particles, what provides significant advantages in terms of thermal effects. Since the spray material is not molten during the process, the thermal influence on the coating and the substrate material is minimized [11].
A CS process plant has been established in the Werner-von-Siemens Centre [12]. **Fig. 2** illustrates the operating principle. Initially, the carrier gas (usually nitrogen or helium) is compressed to 50 bar in the supply tank and heated up to a maximum of 1100 °C. The PM material powder and binder material are then introduced into the supply tank through the powder container. Simultaneously, the mixed powder is accelerated by the carrier gas to supersonic speeds of up to 1200 m/s. Utilizing the spray gun, both materials are propelled onto a carrier substrate, where they are applied in layers. The gas temperature is subsequently reduced down to less than 100 °C at the outlet of the spray gun.

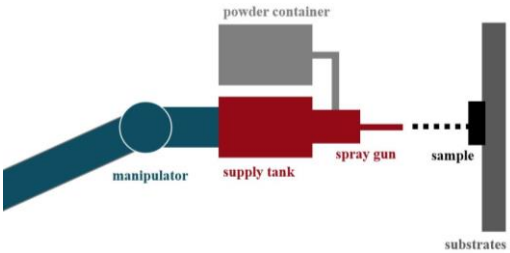

Figure 2: Schematic representation of the cold spray method [13]

2.3 Extrusion (ET)

Compared with micro-crystal sintered magnet prepared by traditional powder metallurgy or the AM-methods mentioned above, the hot-deformed nanocrystalline magnet can obtain anisotropy without magnetic field orientation, and its mechanical properties and corrosion resistance become excellent [14].
Fig. 3 presents a schematic representation of the extrusion process, which involves pressing a heated compact, in this case, an encapsulated NdFeB-billet, through the opening of a die with ceramic and inlet rings using a ram. The compact is contained within a recipient in the form of a thick-walled cylinder, and the die determines the cross-section of the pressed strand [15].

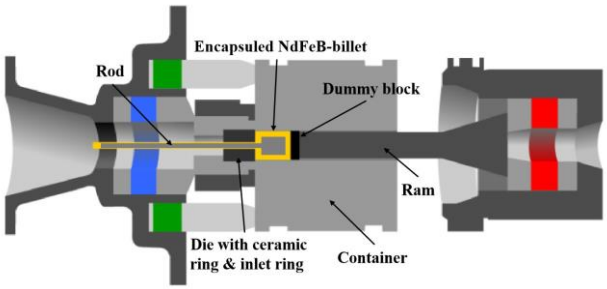

Figure 3: Schematic representation of the extrusion method [15]

2.4 Samples

To assess the magnetic properties and the resulting anisotropy, cubic PM NdFeB samples were produced using the methods illustrated in **Fig. 4**.
The ET samples demonstrate substantial anisotropy attributed to the mechanical shearing occurring during the process. In the contrary, the FDM green parts display a slight anisotropy, achieved through the application of a magnetic field of up to 0.8 T during the manufacturing process. On the other hand, the CS samples exhibit isotropic characteristics due to the absence of a magnetic field during the process.

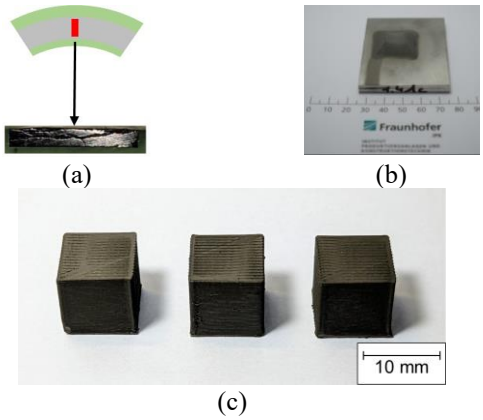

Figure 4: Manufactured samples of (a) extrusion, (b) cold spray and (c) fused deposition modeling.

The corresponding hysteresis curves in the preferred direction and the resulting magnetic characteristics are illustrated in **Fig. 5** and listed in **Tab. 1**, respectively.

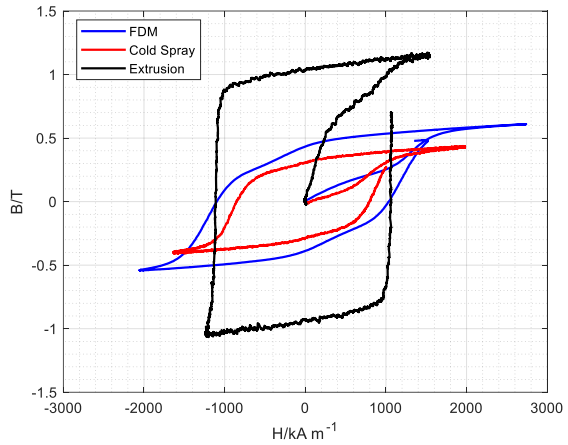

Figure 5: Measured hysteresis curves of manufactured samples

Table 1: Magnetic characteristics of manufactured samples

Manufacturing Methods	Powder	B_r/mT	H_{cJ}/kA m^{-1}
Fused Deposition Modeling	MQA-38-17	435	1099
Cold Spray	MQFP-14-12	307	854
Extrusion	MQU-M-20251-070	1150	1220

3 Design of Magnetizing Coils

The manufactured samples of complete rotors are initially non-magnetic and acquire their polarization through magnetization. The conventional assembly process for PM motors can be intricate and pose potential hazards due to the electromagnetic force exerted by the manufactured and magnetized PMs. Considering of the assembly challenges, it is preferable to magnetize in-situ in a fully or partially assembled device using a pulse discharge magnetizer [16]. Furthermore, a continuous skew effect of an additively manufactured soft-magnetic rotor active part as investigated and analyzed in [17] has also been applied to the samples.

The AM-rotors discussed in this paper can fully benefit from the advantages offered by these approaches, as it enables the realization of theoretically arbitrary pole numbers and continuous skew angles by using special designed magnetizing coils.

3.1 Benchmark and AM-Motors

To investigate the PMs manufactured using the extrusion and AM-methods mentioned above in motors, we used a series-produced electric power steering (EPS) motor as benchmark motor. The rated specifications are derived and presented in **Tab. 2**. The 3D model of the motor, rotor and 2D model is depicted in **Fig. 6** (a)-(c), respectively.

Table 2: Derived rated data of the benchmark motor

U/V	I/A	P_{mech}/W	T/Nm	n/rpm
$12/\sqrt{2}$	32	470	3	1500

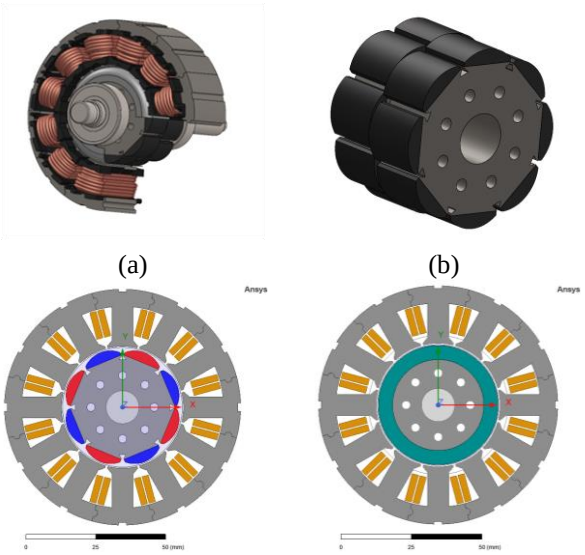

Figure 6: 3D model of (a) EPS motor, (b) EPS rotor and 2D model of (c) EPS motor, (d) AM motor

The EPS-motor designed as a 12-slot and 8-pole servomotor with surface-mounted permanent magnets, has been installed in steering systems of VW group vehicles with the series number 5Q0 909 144 M. Its rotor, measuring 28.6 mm in length and 21.4 mm in radius, comprises two pairs of eight half-moon shaped magnets that are skewed by 7.5° to achieve smooth cogging torque. Consequently, the AM rotors are simulated and manufactured with the same radius to fit into the EPS stators. The permanent magnets are manufactured in cylindrical form with a width of 5 mm, as indicated by the green color in the **Fig. 6** (d).

3.2 Geometry Design

To demonstrate the feasibility of achieving arbitrary pole numbers and skew angles for rotors, customized design of magnetizing coils is essential. In the case of the benchmark motor with 12 slots, magnetizing coils are designed for rotors with 8 and 16 poles. Compared to rotors with 8 poles, where the number of slots per pole and phase q = 1/2 results in the torque being generated by the stator fundamental field wave, the 16-pole rotors with q = 1/4 produce significantly less torque by the second harmonic of the stator field wave. By exploring these combinations, the theoretical skew angle can be calculated as follows:

$$\vartheta_{skew} = k\frac{2\pi}{n_p} \quad mit \;\; n_p = \frac{2pN}{gcd[N,2p]} \qquad (1)$$

In equation (1), k represents a freely selectable factor, n_p donates the period number, p refers to the pole pair number, N stands for the slot number, and gcd is the greatest common divisor.

Due to the increased difficulty in magnetizing anisotropic magnets compared to isotropic magnets, square slots are employed for anisotropic magnets to achieve a more rectangular magnetic field, while round slots are utilized for isotropic magnets to create a sinusoidal magnetic field. The design parameters can be found in **Tab. 3**.

Table 3: Design parameters for magnetizing coils

Coil	Pole number	Magnet type	Skew angle	Slot shape
1	8	Anisotropic	15°	Square
2	8	Isotropic	15°	Round
3	16	Anisotropic /Isotropic	7.5°	Honeycomb

3.3 Electrical and Thermal Design

Typically, capacitive storage devices are employed to generate pulse currents for a pulsed field magnetizer as illustrated in **Fig. 7**. The capacitor is charged slowly by an input side supply to a voltage U_0 and subsequently discharged through a switch over the inductive and resistive load, in this case, the magnetizing coil. The freewheeling diode enables the pulse current to decay exponentially without any overshoot or undershoot once it reaches its maximum value during the half-value time. The design procedure and electric characterization are described in [18].

Based on the designed geometry and construction of the magnetizing coils, the electrical parameters can be determined and presented in **Tab. 4**.

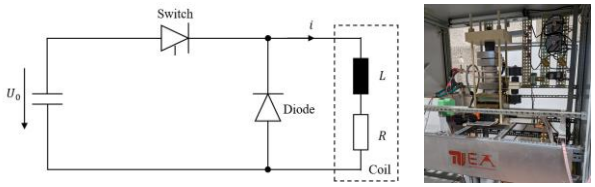

(a) (b)

Figure 7: (a) Schematic representation and (b) the construction of the pulse current circuit with recovery diode

Table 4: Determined parameters for magnetizing coils

Coil	$R/\mathrm{m\Omega}$	L/mH	U_0/V	I_{max}/kA	$\Delta T/\mathrm{K}$
1	14.1	6.6	900	15	40.5
2	24.7	5.3	1250	20	40.6
3	27.3	5.4	1500	22.6	30.0

Furthermore, for safety reasons and to prevent undue thermal stress on the system, it is essential to ensure that the pulse current process causes few losses in the wires. The temperature rise in the magnetizing coil during magnetization can be considered adiabatic in such short time and calculated as follows:

$$\Delta T = \frac{P_v}{C_{th}} = \frac{1}{c_{Cu} m_{Cu}} \int i^2(t) R(t) dt \qquad (2)$$

In equation (2), P_v is the thermal loss and C_{th} is the thermal capacity of the total wire, which can be calculated with the specific thermal heat capacity c_{Cu} and mass of copper m_{Cu}.

Through an iterative calculation process, considering a temperature rise limitation of 40 K, the maximal current I_{max} for each coil can be determined.

3.4 Magnetizing Results

The calculated field lines at the magnetizing points, where the maximal current flows through the coils, are illustrated in **Fig. 8**. The pole transition between poles is clearly visible. In most of the magnet area, the magnetic field strength exceeds 2500 kA/m, which, as indicated in [19], should be sufficient for complete magnetization. The radial flux density in the air gap 0.3 mm above the 8-pole rotors after magnetization was measured by Hall probe and depicted alongside simulated values in **Fig. 9** (a).

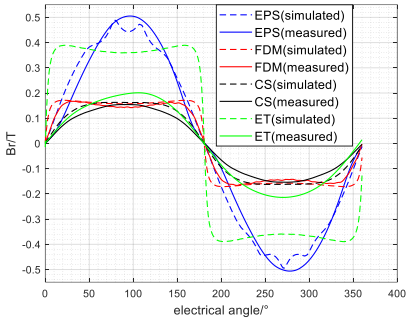

(a)

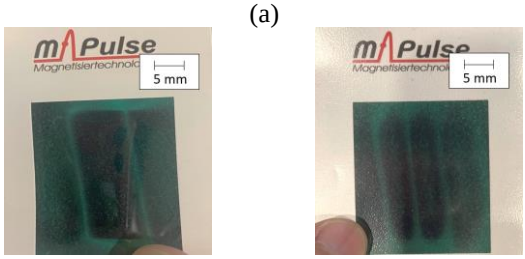

(b) (c)

Figure 9: (a) Simulated and measured radial flux density in the air gap 0.3 mm above the surfaces of 8-pole rotors; Magnetic field distribution of (b) 8-pole and (c) 16-pole CS-rotor

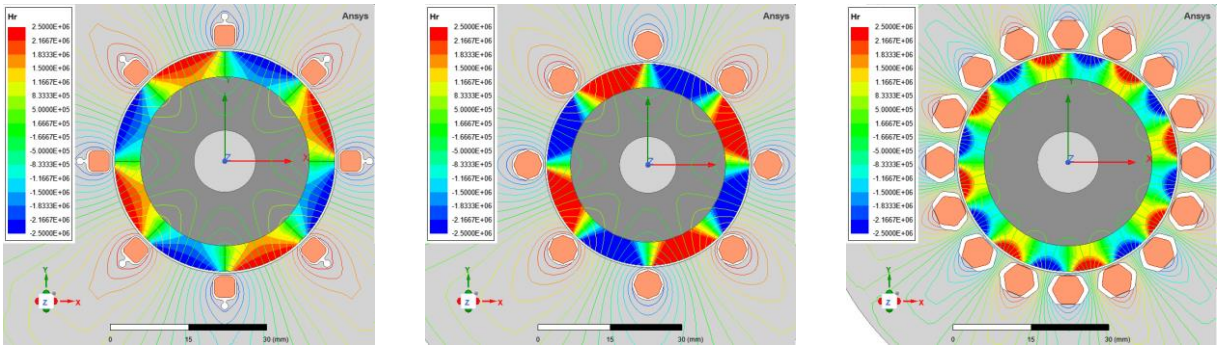

(a) (b) (c)

Figure 8: 2D Magnetostatic FEM simulated field line at the magnetizing point of the (a) 8-pole anisotropic, (b) 8-pole isotropic and (c) 16-pole coil

From **Fig. 9** (a), it is evident that the FDM- and ET-rotors, featuring anisotropic magnets, exhibit a more rectangular flux density pattern, while the CS-rotor displays an almost sinusoidal pattern due to its isotropic behavior. The simulations closely match measurements for all except the ET-rotor, which has lower PM volume due to resin casting to address cracking issues. **Fig. 9** (b) and (c) demonstrate successful magnetization with adjustable continuous skew for 8-pole and 16-pole configurations at the same rotor diameter.

4 Simulation and Investigation

To compare the motor performance, the induced voltage and torque at no-load and load tests were simulated using Ansys Maxwell® for the AM or extruded motors.

4.1 Test bench and manufactured Rotors

As depicted in **Fig. 10**, a setup has been constructed for testing the motor and comprises a target machine and a load machine, which are mechanically coupled with a shaft, along with peripheral equipment to control these machines. This enables the target machine to function as either a motor or a generator.

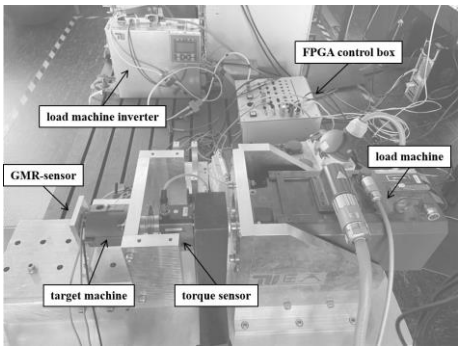

Figure 10: Test bench for testing manufactured motors

To conform to the benchmark stator, the AM and extruded rotors were produced at the same dimensions as the benchmark rotor, as depicted in **Fig. 11**.

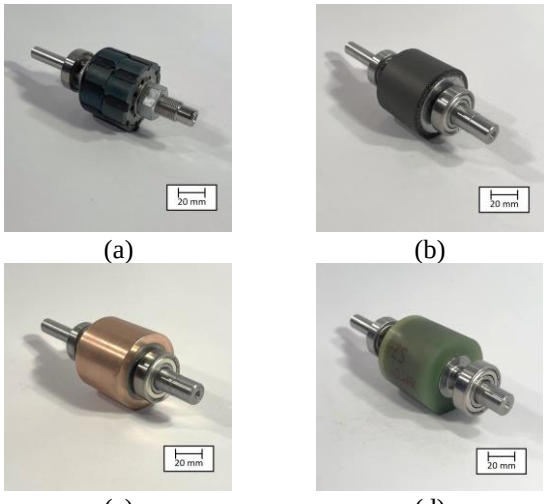

(a) (b)

(c) (d)

Figure 11: Rotors of (a) benchmark, (b) fused deposition modeling, (c) cold spray and (d) extrusion

4.2 Induced Voltage

The induced voltage was simulated and measured in a no-load test with the rotor speed set at 100 rpm. As depicted in **Fig. 12**, the induced phase voltage of AM and extruded motors exhibited sinusoidal forms similar to that of the benchmark motor. However, the amplitude of the induced voltage was significantly lower due to differences in magnetic specifications. Regrettably, the resin layer on the ET-rotor was damaged during stator assembly due to shrinkage. Based on the simulation, the ET-rotor was expected to have the highest amplitude among the manufactured rotors.

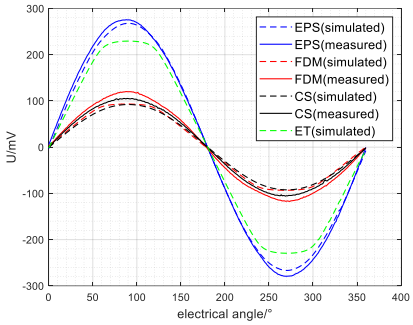

Figure 12: Simulated and measured induced phase voltage at 100 rpm of 8-pole motors

4.3 Torque

The torque was simulated for both no-load and load tests at a constant speed of 100 rpm. In the load test, the stator current was set to 2 A. The resulting torque values for 8-pole motors are shown in **Fig. 13**.

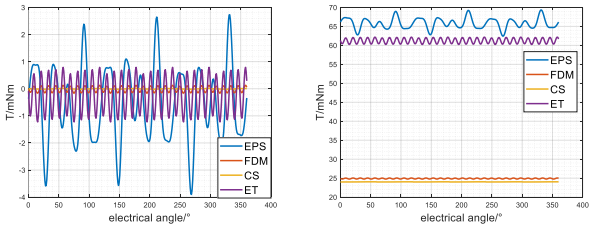

(a) (b)

Figure 13: Calculated torque for (a) the no-load test at 100 rpm and (b) the load test at 100 rpm with stator current of 2 A for 8-pole motors

As a result of in-situ magnetizing and continuous skewing, the AM and extruded motors exhibit reduced cogging torque at no-load test or torque pulsation at load test compared to the benchmark motor. However, the average torque achieved by these motors is lower due to the magnetic properties of the manufactured magnets.

5 Conclusion

5.1 Cost

As the AM and extrusion technology for manufacturing electrical machines has not yet been commercialized, the costs can only be quantitatively estimated and are compared in **Tab. 5**.

Among all the methods, conventional powder metallurgy exclusively requires magnetic powder as the raw material, while FDM and CS require polymer-based and aluminum or copper as binder material, respectively. In extrusion, a steel capsule is necessary to contain the magnetic powder. In terms of plant cost, FDM printers are relatively inexpensive and easily constructed, whereas CS plants are costly and complex. One of the primary advantages of AM and extrusion methods is their higher processing efficiency compared to powder metallurgy.

Table 5: Quantitative estimate on cost

Methods	Material	Plant	Processing
Powder metallurgy	Low	Medium	High
FDM	Medium	Low	Low
CS	Medium	Medium	High
ET	Medium	Medium	Low

5.2 Summary

This paper shows the possibility of manufacturing hard-magnetic materials using FDM, CS and ET methods and successfully generating anisotropy in the magnets during the process. Motors with AM and extruded magnets were designed and simulatively investigated for an EPS-motor. The results indicate that the AM and extruded motors exhibit reduced cogging torque and torque pulsation, due to the in-situ magnetizing and continuous skewing. Importantly, arbitrary pole settings and skew angles have been shown to be realistic possibilities in this context.

6 Acknowledgement

EUROPÄISCHE UNION
Europäischer Sozialfonds

This research was funded by the Investitionsbank Berlin (IBB) with co-financing by the European Regional Development Fund (ERDF).

7 Literature

[1] Lalana, E.: Review Permanent magnets and its production by powder metallurgy, Revista de Metalurgia, Vol. 54 No. 2, 2018, e121, 10 pages

[2] Conrad Electronic: Handbuch 3D-Druck, 2019

[3] Wu, F. *el at.*: Toward Additively Manufactured Electrical Machines: Opportunities and Challenges, IEEE Transactions on industry applications, Vol. 56, No. 2, 2020, pp. 1306-1320

[4] Goll, D. *el at.*: Refining the Microstructure of Fe-Nd-B by Selective Laser Melting, Phys. Status Solidi RRL, Vol. 13, Issue 3, 2019, 5 pages

[5] Li, L. *et al.* Big Area Additive Manufacturing of High Performance Bonded NdFeB Magnets. *Sci. Rep.* 6, 36212; 2016, 7 pages

[6] Lamarre, J. *et al.*: Permanent magnets produced by cold spray additive manufacturing for electric engines, Journal of Thermal Spray Technology, 28, 7, pp. 1709-1717, 2019

[7] Lammers, S. *et al.*: Additive Manufacturing of a Ligh-weight Rotor for a Permanent Magnet Synchronous Machine, 6th International Electric Drives Production Conference in Nuremberg, 2016, 5 pages

[8] Gargalis, L. *et al.*: Additive Manufacturing and Testing of a Soft Magnetic Rotor for a Switched Reluctance Motor, IEEE Access, Vol. 8, 2020, 10 pages

[9] Urbanek S. *at el.*: Additive Manufacturing of a Soft Magnetic Rotor Active Part and Shaft for a Permanent Magnet Synchronous Machine, IEEE Transportation Electrification Conference and Expo (ITEC) in Long Beach, 2018, pp. 668-674

[10] Joamin G. *at el.*: Additive Manufacturing of Metallic and Ceramic Components by the Material Extrusion of Highly-Filled Polymers: A Review and Future Perspectives, MDPI Materials Vol. 11 No. 5, 2018, 36 pages

[11] Braun, T. *at el.*: Evaluation of electric conductivity and mechanical load capacity of copper deposits for application in large winding components for electrical high-voltage machines made with cold spray additive manufacturing, International Thermal Spray Conference Proceedings (ITSC) in Vienna, 2022, pp. 743-749

[12] Werner-von-Siemens Centre, Available at: https://wvsc.berlin (Accessed: 13 September 2023)

[13] Kaltgasspritz-Systeme, Impact Innovations GmbH, Available at: https://impact-innovations.com/produkte (Accessed: 13 September 2023)

[14] Wang, H. *at el.*: Anisotropic Nanocrystalline SmCo5 Permanent Magnet Prepared by Hot Extrusion, IEEE Transactions on Magnetics, Vol. 58, No. 2, 2022, 5 pages

[15] Rüdiger, A. *at el.*: Investigations into the processing and texture of Pr-substituted NdFeB magnets produced by extrusion, Material Forming - ESAFORM 2023, pp. 505-514

[16] Zhilichev, Y. *at el.*: In situ magnetization of isotropic permanent magnets, IEEE Transactions on Magnetics, Vol. 38, No. 5, 2002, 3 pages

[17] Urbanek, S. *at el.*: Effects of Continuous Rotor Skewing in Additively Manufactured Permanent Magnet Rotors, 2020 International Symposium on Power Electronics, Electrical Drives, Automation and Motion, 2020, pp. 662-669

[18] Dinca, C. *at el.*: Chracterization of a 7 kJ Magnetizing Pulsed Circuit for Online Quality Control of Permanent Magnets, IEEE Pulsed Power Conference (PPC) in Austin, 2015, 7 pages

[19] Binder, A.: Design of Coils for Magnetizing Rotors with Surface Rare Earth Permanent Magnets, Proceedings of the International Conference on Electrical Machines (ICEM), 10.-12. Sept.1996, Vigo, p.449-454

Authors


Tong Wu

Tong Wu
Tong Wu received his B. Ing. and M. Sc. degree in Electrical Engineering from University of Shanghai for Science and Technology, together with Hochschule für Angewandte Wissenschaften Hamburg, and Technische Universität Berlin in 2016 and 2019, respectively. Since 2020 he worked as scientific assistant at the Institute of Electrical Drive of Technische Universität Berlin and focused on the additive manufacturing, FEM-simulation, and drive system of electrical machines.


Tobias Neuwald

Tobias Neuwald
Tobias Neuwald received a B. Ing. in Mechanical Engineering and a M. Sc. in Production Technology from the Berlin University of Applied Sciences and the Technische Universität Berlin. Since 2019 he's been working as a Research Associate and since 2021 as the head of the additive manufacturing group within his department at the Fraunhofer-Institute for Production Systems and Design Technology IPK. The focus of his research is the additive manufacturing process chain for metal parts.